Plume Impingement Analysis for the European Service Module Propulsion System

John T. Yim[1]
NASA Glenn Research Center, Cleveland, OH, 44135

Fabien Sibé[2]
Airbus Defense and Space, Les Mureaux, France

and

Nicola Ierardo[3]
ESA/ESTEC, Noordwijk, The Netherlands

Plume impingement analyses were performed for the European Service Module (ESM) propulsion system Orbital Maneuvering System engine (OMS-E), auxiliary engines, and reaction control system (RCS) engines. The heat flux from plume impingement on the solar arrays and other surfaces are evaluated. This information is used to provide inputs for the ESM thermal analyses and help determine the optimal configuration for the RCS engines.

I. Introduction

The Orion Multi-Purpose Crew Vehicle (MPCV) is NASA's next manned spacecraft under development to take humans beyond low Earth orbit. The European Space Agency (ESA) is partnering in the effort by developing and providing the Service Module (SM) for the MPCV architecture.[1] The European Service Module (ESM) will house the MPCV's power, thermal, and propulsion systems. Airbus Defence and Space (AD&S) is the prime contractor under ESA developing the ESM, while NASA as the final customer performs independent verification and validation (IV&V) as necessary including the plume impingement analysis presented in this work.

The ESM propulsion system consists of three engine classes, a 26.7 kN (6000 lbf) Orbital Maneuvering System engine (OMS-E) from Shuttle, eight 490 N (110 lbf) R-4D auxiliary engines, and twenty four 220 N (50 lbf) Reaction Control System (RCS) engines.[2] All of the engines are fed from a common pressure-regulated monomethylhydrazine (MMH) and nitrogen tetroxide (NTO) bipropellant feed system. A diagram showing the general configuration of the ESM and its engines is shown in Figure 1. For all engines, the plume interactions with the spacecraft need to be analyzed to ensure thermal compliance and accurate imparted moments. This work investigates the plume of the OMS-E and the RCS subsystem to assess their impact on the ESM solar arrays, radiators, and other surfaces. Similar efforts have been performed for the previous iteration of the Orion SM.[3,4] The ESM, however, incorporates a different design with the following highlighted changes:[5]

- Using the Shuttle heritage 26.7 kN (6000 lbf) 55:1 area ratio (AR) OMS-E instead of the 33.4 kN (7500 lbf) 150:1 AR Orion Main Engine[6]
- Using the HTV heritage 300:1 AR nozzle extension instead of a 164:1 AR for the auxiliary engines
- Using 220 N (50 lbf) RCS engines instead of 110 N (25 lbf) RCS engines
- Using four rectangular solar arrays instead of two circular Ultraflex arrays

These differences, among several others including engine locations, required a new plume impingement analysis study to be performed. In particular, the simulation results are used to help optimize the RCS engine placement and configuration on the ESM as well as solar array placement and orientation for each burn profile to minimize risk of potential plume induced heat damage and contamination.

[1]Aerospace Engineer, In-Space Propulsion Systems Branch, 21000 Brookpark Rd. MS 86-8, Member.
[2]Aerospace Engineer, Aerodynamics Department, 51-61 Route de Verneuil 78130 Les Mureaux.
[3]ESA Propulsion/GNC Subsystem Manager, Keplerlaan 1 NL-2200 AG Noordwijk.

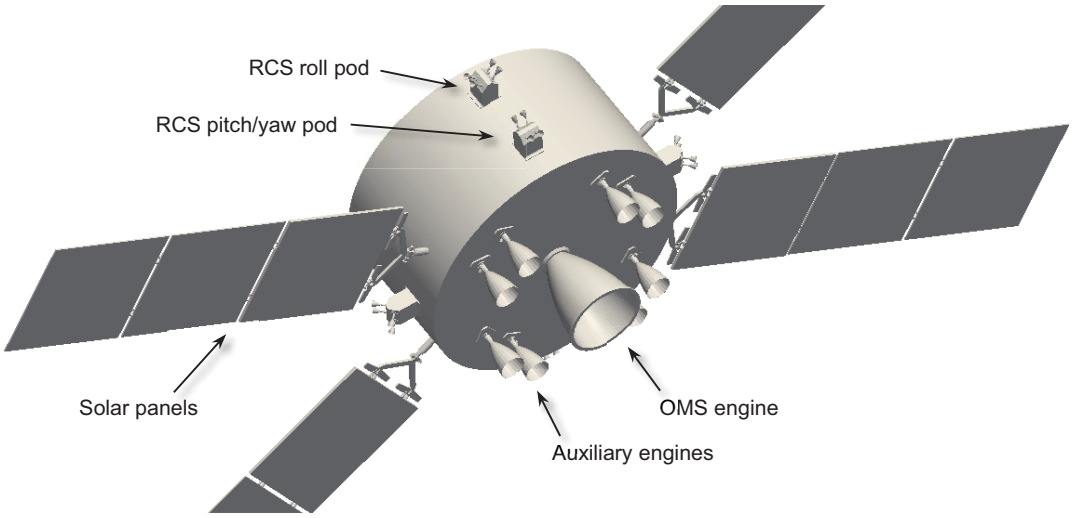

Figure 1: Depiction of ESM with the 24 RCS engine configuration.

II. Model Descriptions

Several models were applied to assess the effects of plume impingement on the ESM solar arrays and other surfaces. Two codes were used by AD&S to analyze the ESM RCS, OMS-E, and auxiliary engine plumes while another two sets of codes were used for the NASA IV&V analysis to examine the plume properties of the ESM RCS engines and the OMS-E. These codes involve different approaches including ray tracing, method of characteristics, and direct simulation Monte Carlo (DSMC) methods.

The first AD&S code used is the RAYJET simulator, which has been used for plume simulations of the automated transfer vehicle (ATV) including plume effects on the International Space Station (ISS) during rendezvous operations. RAYJET uses a ray tracing method where rays are thrown about the plume axis from a point source with properties simulated by a fitting function deduced from Monte Carlo simulations. Rays intersecting a surface are determined and the properties at the surface location are calculated. This includes normal pressure, shear pressure, and the heat flux. The properties are dependent on the flow regime whether continuum or free molecular flow; a bridging method, after Matting, well adapted to transitional flow is used here.[7]

The second model used by AD&S is the Internal External Monte Carlo (IEMC) which is based on the DSMC method. The DSMC method is a particle-based gas flow simulation technique which is derived from principles of kinetic theory. A large population of simulated particles is tracked through the computational domain, with a combination of deterministic particle movement routines and probabilistic binary collision routines, in order to simulate underlying physics in the governing Boltzmann equation. Other DSMC implementations have been successfully used for plume flow and plume impingement studies.[8-9] For example, the DSMC Analysis Code (DAC) has been applied to model plumes for several different programs including plume impingement on the ISS, the Orion SM RCS engines, and the Altair lunar lander ascent engine among others.[10-12] These efforts have shown that DSMC is a viable method to simulate and analyze plume flows and resulting plume impingement. IEMC uses the variable hard sphere (VHS) collision model and the energy transfer treatment between molecules and walls is modeled after Borgnakke and Larsen.[13] The code includes MPI parallelization, a local time step adaptation and can take into account hybrid tetrahedral and hexahedral meshes and several molecules species.

The Reacting And Multi-Phase (RAMP2) / PLume IMPingment (PLIMP) program combination is a NASA heritage plume analysis model that is applied to the ESM engines. RAMP2 is an axisymmetric method-of-characteristics based code that calculates the plume flowfield beginning from the engine nozzle throat to the exit plane within a user supplied nozzle profile.[14] It also calculates the plume flowfield expansion beyond the exit plane. It has the capabilities to account for nozzle boundary layers, multi-phase flow, and flow chemistry among other options. A Chemistry Equilibrium with Applications (CEA) code equivalent is used to generate the flow properties which are input into RAMP2. The RAMP2 flowfield can be used as an input to the PLIMP code to subsequently calculate forces, moments, pressures, heating rates, and species contamination on surfaces specified by the user.[15] PLIMP has the capability to apply the appropriate flow regime from turbulent viscous flow to free molecular, to determine the appropriate surface impingement properties. RAMP2 and PLIMP have been used for a number of plume impingement studies, including a previous version of the Orion SM as noted above. Other projects have also

used RAMP2 and PLIMP, including Shuttle RCS and solid rocket boosters, Space Launch System (SLS) solid rocket boosters, and the Green Propellant Infusion Mission (GPIM) monopropellant thrusters among others.[16-18]

The second method used by NASA is the Hypersonic Aerothermodynamics Particle (HAP) code. The HAP code is a general Cartesian implementation of DSMC, with features including dynamic grid adaptation; shared memory parallelization; and options to import externally defined surface geometries or to automatically generate triangulated surfaces based on analytical geometry definitions.[19] In particular, a useful ability of the code is the use of a collision limiter scheme with a gradient-based local time step adaptation to selectively reduce numerical errors from multiple sources (e.g. incomplete equilibration, operator splitting, finite collision separation) within regions which are especially prone to inaccuracy.[20] This allows for efficient calculation of the low Knudsen number regions of the flow without being overly diffusive. With this capability, an inflow boundary applied at the engine exit plane was able to be implemented. The CEA program is used to generate the species composition, plume density, temperature, and flow velocity at the appropriate area ratios to be used for the inflow boundary conditions. HAP then calculates the resultant expansion flow of the engine plume. This approach was also used for the plume impingement analysis for the GPIM project.[18] A geometry model of the ESM spacecraft was imported into the program and the particle flux and heat transfer were calculated at the surfaces. For the OMS-E case for spacecraft interaction, symmetry planes were utilized in the lateral directions to reduce the computational requirements. Due to the inherent asymmetry of the RCS engine positions and orientation vectors on the ESM, no symmetry advantages were applied for that particular model. Typical simulations run for this required on the order of two to three million simulated particles.

III. Results and Discussion

A. RCS plumes

For the RCS, a number of cases were examined with different engine and solar array orientations. These cases were run to find the optimal configuration of RCS engines that could accommodate all of the necessary burn maneuvers while remaining within the thermal limits of the solar panels. Two RCS configurations were assessed, one with 24 engines, eight each for roll, pitch, and yaw, as shown above in Figure 1. The other configuration used a minimal 16 engine configuration, where the upper roll pods were removed and the engines on the lower pods were canted azimuthally to produce roll torques. The RCS configurations utilize redundant engines at each location. Only one engine of each pair is nominally operated, but in certain contingency abort scenarios both strings may be operated simultaneously. For the analyses presented here, only one RCS engine firing at a time is examined except for the abort scenario where two engines firing are evaluated.

Several configurations also exist for the solar arrays. They are always attached to the SM at the same location. They can be canted vertically with respect to the center axis of the SM nominally between -35° (towards the OMS-E) and 25°. For an extended OMS-E burn, they can also be canted at 55°. They also have the capability to swivel 180° around the long axis of the solar array. Finally, they are also folded up and stowed against the body during launch and aborts. For abort scenarios, the stowed solar array configuration was modeled, while for nominal in-flight operations the deployed configurations were assessed to find the optimal orientation within operational constraints that minimizes plume impingement.

For each configuration, the potential operation of the RCS engines was defined by the project guidance, navigation, and control (GNC) team. A set of operational profiles defined what engines could be fired along with burn durations and duty cycles. These engine burn durations and duty cycles were then used by the thermal team to define what the allowable heat flux limits were for the solar arrays. These were determined through a thermal model and the allowable temperature limits of the array, which were primarily restricted by the adhesive material. The heat flux allowables were delineated between the panel surface and the panel edges. The two, however, are taken into account together, and the limits for both are dependent on the state of the other; a curve was provided to define the combined limits for both for each engine firing scenario.

A sample case is used to highlight the comparisons among the different analysis codes and methods. A single roll RCS jet is modeled to impinge on a deployed solar array with each of the codes. The results, shown in Figure 2, show generally good comparison among the different methods. The RAMP2/PLIMP results are the most disparate from the others, and this is typically seen in the other cases examined as well where the RAMP2/PLIMP calculated heat fluxes can be up to an order of magnitude higher than those calculated from the other methods. The specific reason for this discrepancy is unclear. In general, the best comparison is often found between the two DSMC codes across the different plume cases examined in this work. It should be noted that these and all subsequent heat flux results presented here are from direct plume impingement effects only. Radiative heating from the plume, engines, and other sources of heat are not considered here.

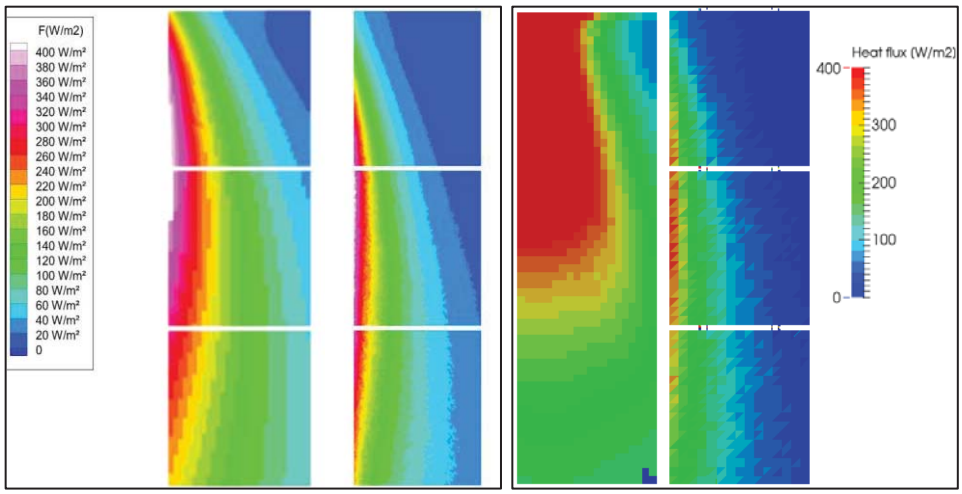

Figure 2: Sample heat flux profiles on a solar array for RAYJET (left), IEMC (left middle), RAMP2/PLIMP (right middle), HAP (right).

Table 1: Maximum heat flux on the solar panel face shown in Figure 2.

Model	Peak heat flux [W/m2]
RAYJET	412
IEMC	410
RAMP2/PLIMP	736
HAP	373

The stowed array configuration is examined first. The RCS engines would only fire for a contingency abort scenario; nominally they would remain off. It is possible that both RCS strings would operate to provide extra torque in the high stressing abort conditions. The thermal worst case, then, would be two engines side-by-side simultaneously firing, particularly two adjacent engines nestled between two stowed arrays. For the 24 engine configuration, the peak heat flux on the solar panel edges was around 0.8 kW/m^2 as calculated by the two DSMC codes, while the surface heat flux was closer to 0.1 kW/m^2. The IEMC results are shown in Figure 3. The RAMP2/PLIMP results, on the other hand, estimated a peak heat flux over an order of magnitude higher on the edges. However, even this heat flux was well within allowable limits as determined from thermal analysis. For the abort scenarios, the longest continuous RCS engine burn was estimated to be five seconds long, while pulse mode behavior did not exceed a 10% duty cycle or 100 ms pulse widths. Thus, for the abort scenarios, the allowable heat flux was relatively high, in the tens of kW/m^2. This is well above the predicted heat fluxes from any of the different plume models and therefore not likely a concern. The roll engines in the upper pods are situated further away from the stowed arrays, though there is a greater view factor to the rear side of the panels. The panel heat flux was found to be higher and the edge heat flux lower, but both fluxes were also well below the allowable thermal limits.

The abort scenarios with the 16 engine configuration were worse, as would be expected since the engines, in close proximity to the stowed arrays, are now canted preferentially towards one of the arrays. The maximum heat flux on the edge predicted by the worst-case RAMP2/PLIMP model is now nearly 50% greater than the 24 engine configuration. However, these values still remain below the allowable heat flux for this burn profile and array configuration.

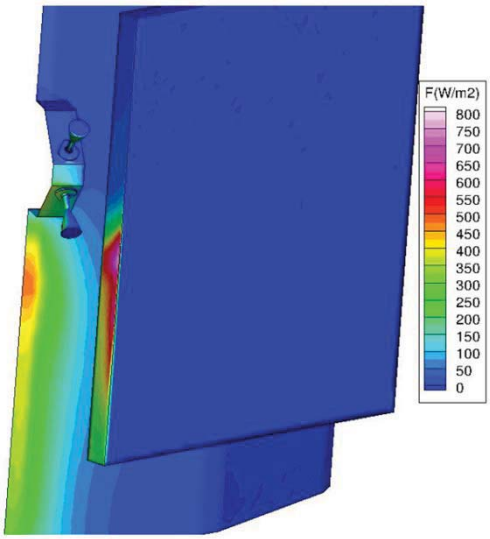

Figure 3: Heat flux profiles for the stowed solar array case calculated with IEMC.

For the deployed array configurations, a number of selected RCS engine, burn duration, and solar array orientation combinations were examined. These can be grouped into three general categories to simplify description. The first, involving RCS attitude control in free flight, allows the greatest range of combinations of engine operation and solar array orientation, but operates at a very low duty cycle with short burn durations. The second, roll control during OMS-E or auxiliary engine burns, use only the roll RCS engines with the potential for the solar arrays to be canted up towards the roll engines and can use higher burn durations and duty cycles. The third, providing ΔV capability, use only translational maneuver burns and the solar arrays in the zero canted orientation. Here, the RCS burn durations can be as high as 80 seconds continuous. The first category, free flight, was found to tolerate very high thermal fluxes, over 100 kW/m^2, due to the very low duty cycle and pulse widths and so those will not be described in more detail herein other than to note that all cases were analyzed and found to have more than sufficient thermal margin for both the 24 and 16 engine RCS configurations.

For RCS roll control during an OMS-E burn, the arrays will be canted 55° away from the OMS-E during OMS-E operation due to structural load considerations on the arrays. Unfortunately, this places them much closer to the roll pods for the 24 engine RCS configuration, where the roll engines are located in the upper pod as depicted in Figure 1. However, results from RAYJET, RAMP2/PLIMP, and HAP all have a margin of at least 3x on the allowable heat flux for the RCS duty cycles and pulse widths for this case. During auxiliary engine burns, the arrays can be canted as high as 25°, and after a survey of different solar array orientations, this was indeed the worst from a plume impingement perspective, as shown in Figure 4. Even here, though, the margins are above a factor of two for both the solar cell and edge heat flux within the allowable curve and not a cause for concern. In contrast, for the 16 engine RCS configuration, the allowable heat fluxes for both the 55° cant OMS-E roll control case and the 25° auxiliary roll control case are well exceeded by a factor of ten and two, respectively. Results from RAMP2/PLIMP, HAP, and IEMC also showed the same conclusions as the RAYJET results do. The RAYJET results shown in Figure 4 already incorporate a built-in margin of 2x.

Finally, perhaps the most stressing case found from a plume induced heating on the arrays are from the RCS ΔV scenarios. Again, this is due to the potential long continuous burn durations which consequently reduce the acceptable heat flux on the arrays. In addition, depending on the translation maneuver, for the 24 engine configuration, either the pitch/yaw engines on the lower pods or the roll engines on the upper pods can be firing. In this scenario, however, power generation is not pressing for the duration of the burn and the solar arrays can be oriented to any position to minimize the plume impingement, so only one acceptable array configuration needs to be found for each maneuver. After assessing a number of solar array orientations, the best configuration from a heat flux standpoint was found to be a 0° cant with a 90° rotation about the array long axis for both pitch/yaw and roll maneuvers. Figure 5 shows some sample results of the RCS ΔV case with different simulation models, 24 vs. 16 RCS engine configurations, solar array rotation angles, and selected firing RCS engine. The margin on the cell side heat flux for a 24 engine roll engine is slightly under 2x for both the RAYJET and HAP results, but otherwise the 24 engine configuration is well within the limits. The 16 engine configuration is seen to have little margin or even exceed the solar array heat flux limits for these cases.

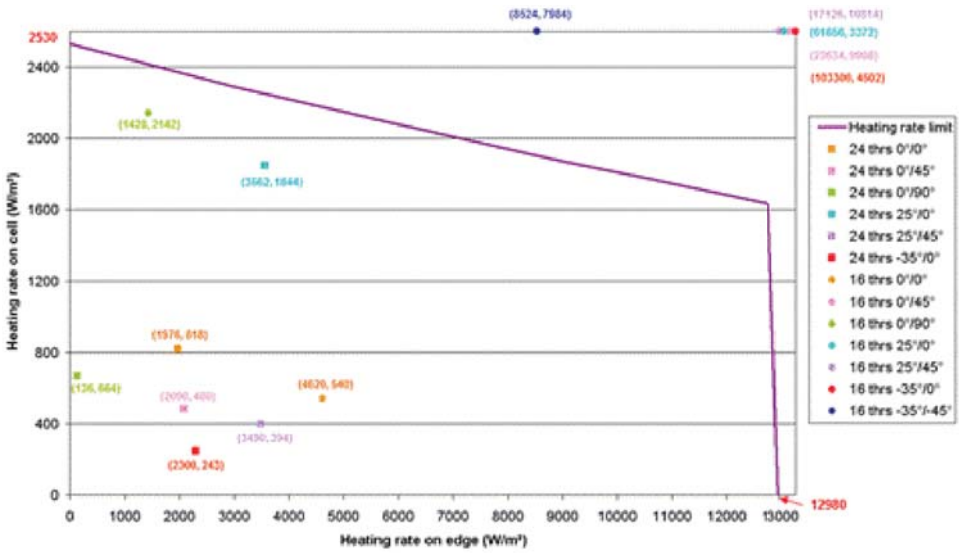

Figure 4: RCS roll control firing plume heat flux on solar arrays for different array orientations during an auxiliary engine maneuver as calculated with RAYJET.

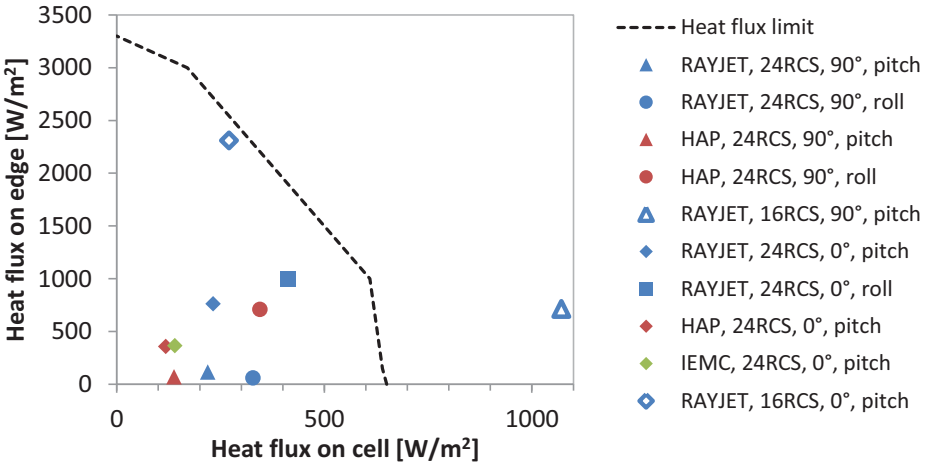

Figure 5: RCS ΔV firing scenario heat fluxes with different simulation models, RCS configurations, solar array rotations, and select RCS engine.

Overall, the 24 engine RCS configuration was found to provide lower, and acceptable, heat fluxes than the 16 engine configuration which had a few scenarios were the heat fluxes exceeded, sometimes greatly, the allowable limits. Though not discussed in much further detail here, when taking into account other factors that influence RCS configuration, including GNC performance, overall mass impact, and reliability and fault tolerance, the 24 engine configuration was found to be a preferable choice for the overall ESM design.

B. OMS-E plume

The cases examined here investigate the OMS-E operating at nominal conditions with the NASA models. This includes the thrust vector control operating with a zero degree gimbal position. The solar arrays will likely be canted 55° away from the OMS-E during these burns as described above, but a zero degree cant is modeled as a worst-case bound. The HAP and RAMP2 results of the plume flowfield density are shown in Figure 6. There are some noticeable differences between the RAMP2 flowfield and the HAP flowfield, but that is explainable in part that the RAMP2 flowfield is calculated disregarding any physical obstructions apart from the engine nozzle. The spacecraft geometry is introduced through the application of PLIMP, whereas the HAP results include the effects of the spacecraft on the plume flowfield. That may explain why the downstream portion of the plume is similar for both, yet the flow near the SM body and solar arrays are somewhat different.

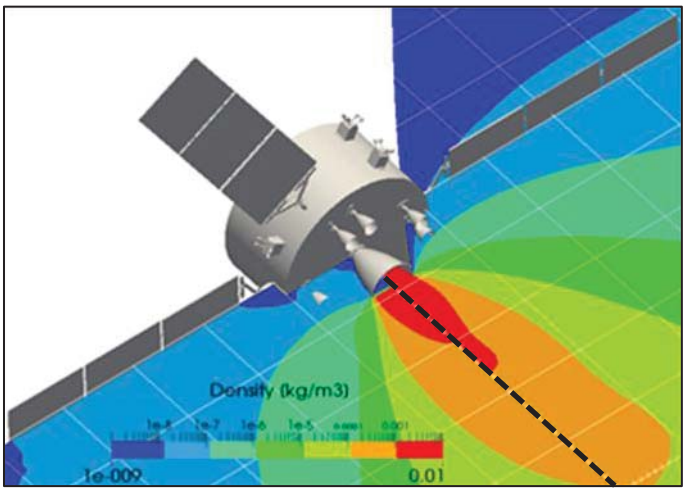

Figure 6: OMS-E plume density profiles calculated using HAP (left) and RAMP2 (right).

The RAMP2 results are then used in the PLIMP program to produce the resultant heat flux on the ESM surfaces, while the HAP program also produces the surface heat flux. The heat fluxes on the ESM calculated by HAP are shown in Figure 7. The maximum heat flux calculated here on the 0° canted solar array is around 20 W/m^2, while for the PLIMP results, the maximum heat flux on the solar array panel faces was calculated to be closer to 570 W/m^2. The HAP results are more than an order of magnitude lower than the PLIMP results above. In general, the RAMP2/PLIMP results tend to exhibit a much higher heat flux on surfaces at high angles from the thrust axis, especially in the backflow or upstream regions. It is suspected that the HAP results are likely closer to the actual values as the backflow region tends to be in the rarefied flow regimes where the DSMC method is expected to be more accurate than the continuum-based method-of-characteristics solver of RAMP2. This has also been seen in past work and was also observed in the previous RCS simulation results. For the nominal 55° canted solar arrays, the heat fluxes are notably lower as would be expected. The peak heat flux on the solar panel edges are around 120 W/m^2. The faces of the array panels were calculated to have zero heating from the plume in this 55° case, as the panels are aligned essentially parallel to the direction of the plume flow.

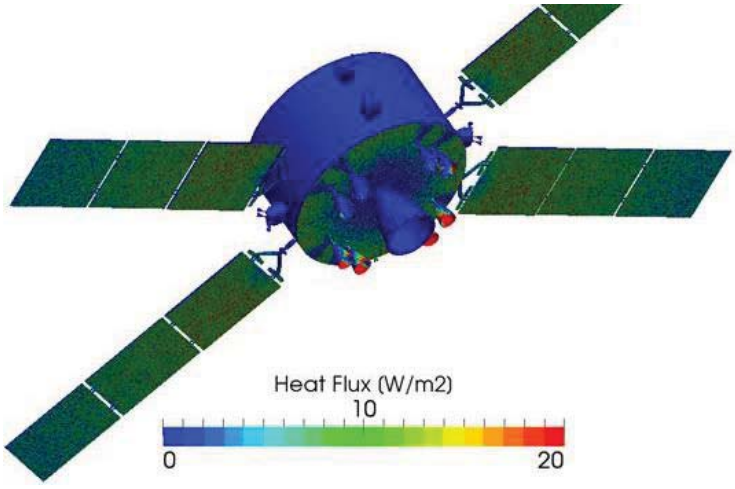

Figure 7: Heat flux from OMS-E plume impingement calculated using HAP.

C. Auxiliary engine plumes

The auxiliary engines were analyzed using the AD&S models, namely IEMC. Here, the primary target of concern was not the solar arrays, but the aft end of the ESM and the OMS-E and auxiliary engine nozzles. The eight auxiliary engines firing by themselves were examined, as well as the combined case where the OMS-E fires as well in an abort scenario. Heat flux plots for these cases are shown in Figure 8 and the corresponding peak values are shown in Table 2. The results between the auxiliary only and the OMS-E and auxiliary together show that the plume

impingement heat flux are not a simple superpositioning of the independent plumes. Rather, this indicates there is non-negligible interaction between the OMS-E and the auxiliary engine plumes. Also shown in Table 2 are the results from HAP simulations of the OMS-E only case as described above in the previous section. The agreement between the two DSMC codes correlates well.

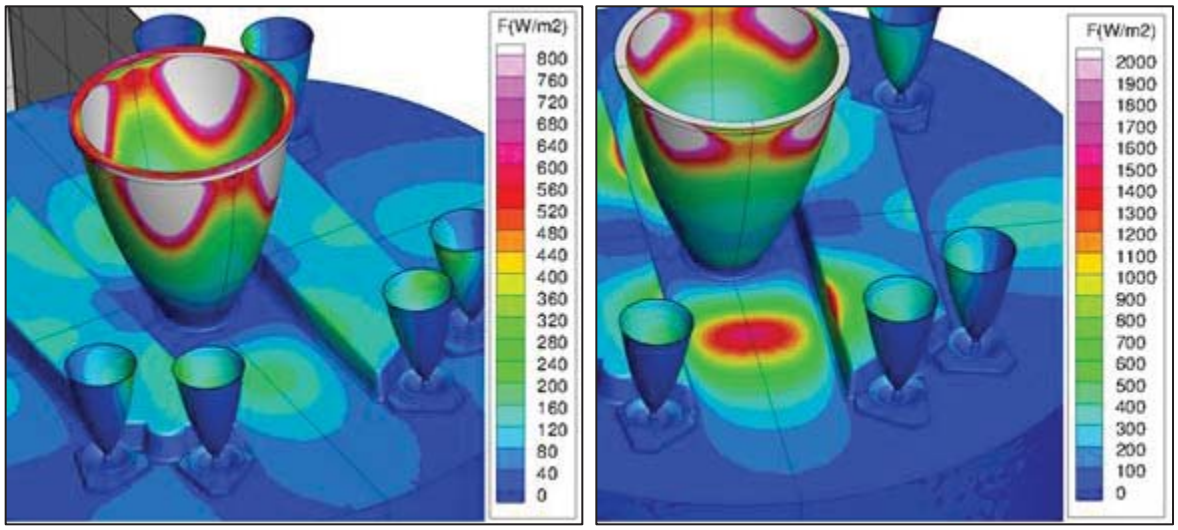

Figure 8: Heat fluxes from all eight auxiliary engines firing (left) and all eight auxiliary engines and the OMS-E firing (right) as calculated with IEMC.

Table 2: Maximum heat flux values on ESM aft end surfaces as calculated by IEMC for different firing engine scenarios.

Firing engines	Peak heat flux [W/m^2]		
	OMS-E nozzle	AUX nozzles	Aft end
OMS-E + 8 AUX	10100	615	1560
8 AUX only	7200	340	225
OMS-E only	--	160	52
OMS-E only (HAP)	--	155	40

IV. Conclusion

The plume impingement analysis for the ESM played an important role in determining the design and impacts of the ESM propulsion system. Several different methods were applied to assess the extent of plume induced heat flux to sensitive surfaces, particularly the solar arrays. The OMS-E, auxiliary engines, as well as the entire range of RCS configurations, firing scenarios and burn durations, along with solar array orientation and appropriate thermal flux limits depending on the case was examined. With some adjustments to the design and operation, a robust solution was found that satisfied plume impingement impacts with sufficient margin to proceed with the ESM design. Modeling efforts from both NASA and Airbus and incorporating a cross-system analysis including GNC, power, and thermal were necessary to find a design solution that closed and met system requirements and needs.

Acknowledgments

The authors would like to thank the support of the ESM project management as well as propulsion, GNC, power, thermal, and system engineering teams from NASA, ESA, and AD&S.

References

[1]Berthe, P., Schubert, K., Grantier, J., Pietsch, K., Angelillo, P., and Price, L., "The Multi-Purpose Crew Vehicle European Service Module: a European Contribution to Human Exploration", *AIAA SPACE 2013*, San Diego, CA, AIAA-2013-5477, September 2013.

[2]Jäger, M., Pitt, R., Ierardo, N., and Dickens, K., "MPCV Service Module Propulsion Subsystem", *Space Propulsion 2014*, Cologne, Germany, 2969277, May 2014.

[3]Wang, X. J. and Yuko, J. R., "Thermal Analysis on Plume Heating of the Main Engine on the Crew Exploration Vehicle Service Module," *Thermal and Fluids Analysis Workshop (TFAWS) 2007*, Warrensville Heights, OH, TFAWS 07-1012, NASA/TM—2007-215049, September 2007.

[4]Wang, X. J., Lumpkin, F. E., Gati, F., Yuko, J. R., and Motil, B.J., "Orion Service Module Reaction Control System Plume Impingement Analysis Using PLIMP/RAMP2," *47th AIAA Aerospace Sciences Meeting and Exhibit*, Orlando, FL, AIAA-2009-0834, January 2009.

[5]Hickman, H. K., Dickens, K. W., Madsen, J. M., Gutkowski, J. P., Ierardo, N., Jäger, M., Lux, J., Freudenberger, J. L., and Paisley, J., "Evolution of MPCV Service Module Propulsion and GN&C Interface Requirements", *AIAA Propulsion and Energy 2014*, Cleveland, OH, July 2014.

[6]Millard, J., Reed, B., "Implementation of the Orbital Maneuvering System Engine and Thrust Vector Control for the European Service Module," *AIAA Propulsion and Energy 2014*, Cleveland, OH, July 2014.

[7]Matting, F. W., "Approximate Bridging Relations in the Transitional Regime between Continuum and Free-Molecule Flows", *Journal of Spacecraft*, Vol. 8, No. 1, January 1971.

[8]Ketsdever, A. D., Lilly, T. C., Gimelshein, S. F., and Alexeenko, A. A., "Experimental and Numerical Study of Nozzle Plume Impingement on Spacecraft Surfaces," *24th International Symposium on Rarefied Gas Dynamics*, Bari, Italy, AIP Conf. Proc. Vol. 762, pp. 367-372, July 2004.

[9]Kannenberg, K. C., and Boyd, I. D., "Three-Dimensional Monte Carlo Simulations of Plume Impingement," *Journal of Thermophysics and Heat Transfer*, Vol. 13, No. 2, pp. 226-235, 1999.

[10]Lumpkin, F. E., III, Marichalar, J., Stewart, B. D., "High Fidelity Simulations of Plume Impingement to the International Space Station," *33rd JANNAF Exhaust Plume and Signatures Subcommittee Meeting*, Monterey, CA, December 2012.

[11]Prisbell, A., Marichalar, J., Lumpkin, F., and LeBeau, G., "Analysis of Plume Impingement Effects from Orion Crew Service Module Dual Reaction Control System Engine Firings," *27th International Symposium on Rarefied Gas Dynamics*, Pacific Grove, CA, AIP Conf. Proc. Vol. 1333, pp. 595-600, July 2010.

[12]Marichalar, J., Prisbell, A., Lumpkin, F., and LeBeau, G., "Study of Plume Impingement Effects in the Lunar Lander Environment," *27th International Symposium on Rarefied Gas Dynamics*, Pacific Grove, CA, AIP Conf. Proc. Vol. 1333, pp. 589-594, July 2010.

[13]Borgnakke, C. and Larsen, P. S., "Statistical Collision Model for Monte Carlo Simulation of Polyatomic Gas Mixture," *Journal of Computational Physics*, Vol. 18, Is. 4, pp. 405-420, August 1975.

[14]Smith, S. D., "High Altitude Chemically Reacting Gas Particle Mixtures," NASA CR-171826, August 1984.

[15]Bender, R. L., Somers, R. E., Prendergast, M. J., Clayton, J. P., and Smith, S. D., "1991 Version of the Plume Impingement Computer Program," NASA CR-194192, October 1991.

[16]Rochelle, Wm. C., Hughes, J. R., DeVenezia, J., Bouslog, S. A., Leahy, K. S., and Fitzgerald, S. M., "Plume Impingement Heating to International Space Station (ISS)," *30th AIAA Thermophysics Conference*, San Diego, CA, AIAA-95-2132, June 1995.

[17]Mehta, M., Williams, B., Putnam, G. C., and Smith, S. D., "Numerical Modeling of Solid Rocket Motor Plumes," *2012 Thermal and Fluids Workshop*, Pasadena, CA, August 2012.

[18]Yim, J. T., Reed, B. D., and McLean, C. H., "Green Propellant Infusion Mission Plume Impingement Analysis," *49th AIAA/ASME/SAE/ASEE Joint Propulsion Conference & Exhibit*, San Jose, CA, AIAA-2013-3850, July 2013.

[19]Burt, J. M., Josyula, E., and Boyd, I. D., "Novel Cartesian Implementation of the Direct Simulation Monte Carlo Method," *Journal of Thermophysics and Heat Transfer*, Vol. 26, No. 2, pp. 258-270, 2012.

[20]Burt, J. M. and Josyula, E., "Efficient Direct Simulation Monte Carlo Modeling of Very Low Knudsen Number Gas Flows," *52nd AIAA Aerospace Sciences Meeting*, National Harbor, MD, AIAA-2014-0697, January 2014.